Results in Physics 14 (2019) 102414

Contents lists available at ScienceDirect

Results in Physics

journal homepage: www.elsevier.com/locate/rinp

Linear and nonlinear optical properties of donors inside a CdSe/ZnTe core/shell nanodot: Role of size modulation

A. Chafai[a], I. Essaoudi[a,c], A. Ainane[a,b,c,*], R. Ahuja[c]

[a] Laboratoire de Physique des Matériaux et Modélisation des Systèmes, (LP2MS), Unité Associée au CNRST-URAC 08, University of Moulay Ismail, Physics Department, Faculty of Sciences, B.P. 11201, Meknes, Morocco
[b] Max-Planck-Institut für Physik Complexer Systeme, Nöthnitzer Str. 38, D-01187 Dresden, Germany
[c] Condensed MatterTheory Group, Department of Physics and Astronomy, Uppsala University, 75120 Uppsala, Sweden

ARTICLE INFO

Keywords:
Shallow donor
Core/shell materials
Optical absorption coefficient
Refractive index
Size effect
Quantum dots

ABSTRACT

The optical absorption coefficient (OAC) and the refractive index (RI), related to a confined donor, were theoretically investigated by the mean of the density matrix formalism. In order to obtain the $1s - 1p$ donor transition energy a variational calculation, within the context of the effective-mass approach, was deployed. Our numerical results exhibit the possibility to modulate the electronic and optical properties of confined donors by tailoring the inner and outer radii of the core/shell heterodot. Further, we have obtained that the nanodot size shrinking leads, for very small values of core radius, to reduce the magnitude of the total absorption coefficient resonance peak. It was also obtained that the resonance peak position of the absorption coefficient is redshifted with increasing the core radius for a fixed shell thickness. The same situation occurs when reducing the thickness of the shell material for a fixed core size.

1. Introduction

It is widely recognized, nowadays, that the progress of electronic and opto-electronic devices depends on the level of understanding fundamental chemical and physical properties of low dimensional structures. Thus, in the last few decades, intense research activity worldwide concerning the behavior of matter at nanoscales was conducted. However, though our current appreciation of nanosized particles has lead us to develop various appliances, examples include light-emitting diodes in television screens, photodetectors in digital cameras, or even quantum dot single-photon source used in the area of quantum information, “controlling” the properties of nanoscaled materials still the greatest challenge of scientists.

According to the fact that nanoscale semiconductors optical behavior is ultimately related to their electronic properties, let us start with a short review of the shrinking size and external fields impacts on confined donors energy behavior. For instance, one can mention the work of Cristea [1] emphasizing the impacts of the donor position and an external electric field on the core/shell nanodot energy spectrum. This study, performed by a finite element approach, investigates also the role of the ZnS/CdSe shape on the confined donor electronic properties. Further, using a finite-difference calculation Souza and Alfonso [2] have examined the change of the binding and the transition energy of donors against the nanodot radius and the magnetic field intensity. Then again, Causil et al. [3] have treated the case of an impurity donor in a cylindrical type-II quantum dot. Their theoretical study, based on a variational Rayleigh–Ritz approach, reveals that the donor ground state binding energy as well as the lowest excited states are size controlled. Besides, the examination of energy levels of donors inside a GaAs/Al_xGa_{1-x}As/AlAs inhomogeneous spherical quantum dot was the subject of Ref. [4]. It was established that the $Al_xGa_{1-x}As$ layer drastically affects the confined donor energy levels. On the other hand, considering a spherical CdSe/ZnS/CdSe core/shell/shell heterodot, Stojanović and Kostić [5] have investigated the spatial parameters influence on single donor states energy. Their results exhibit that for core radius values greater than a critical radius, size effects disappear and energy values tend to those characteristic of the bulk CdSe case. Furthermore, combining fourth-order Runge-Kutta method and variational approaches, Kes et al. [6] have studied the quantum confinement effects on donors inside AlAs/GaAs/$Al_{x_1}Ga_{1-x_1}$As/GaAs/$Al_{x_2}Ga_{1-x_2}$ layered wire. Their model confirms the fact that donors energy is also sensitive to the donor position and external fields. Polaronic impacts on the donor binding energy is treated by El Haouari et al. [7]. Their investigation shows the existence of a competition between polaronic and

* Corresponding author at: Laboratoire de Physique des Matériaux et Modélisation des Systèmes, (LP2MS), Unité Associée au CNRST-URAC 08, University of Moulay Ismail, Physics Department, Faculty of Sciences, B.P. 11201, Meknes, Morocco.
E-mail address: a.ainane@fs-umi.ac.ma (A. Ainane).

https://doi.org/10.1016/j.rinp.2019.102414
Received 23 April 2019; Received in revised form 21 May 2019; Accepted 1 June 2019
Available online 11 June 2019

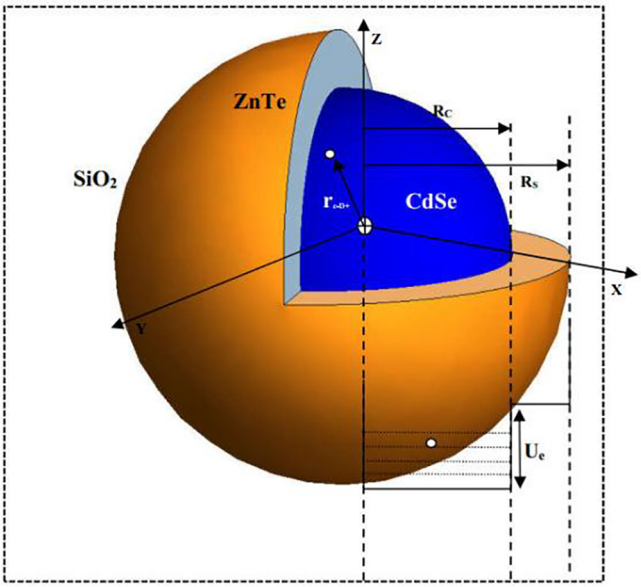

Fig. 1. Schematic illustration of a single centered donor inside a spherical-like core/shell nanodot.

Table 1
The used numerical parameters [37,38].

	CdSe	*ZnTe*	The used parameters
E_g	1.750 eV	2.200 eV	
ε_r	$\varepsilon_1 = 10.600$	$\varepsilon_2 = 9.700$	$\tilde{\varepsilon} = 10.140$
$\frac{m_e^*}{m_0}$	$m_1^* = 0.130$	$m_2^* = 0.150$	$\tilde{m}_e^* = 0.139$
Γ_0			4.00010^{-3} fs
Electron affinity	$E_{ea} = 4.950$ eV	$E_{ea} = 3.680$ eV	

size effects. Moreover, using a variational calculation, Chafai et al. [8] have studied the charge carriers localization influence on single donor binding energy. It was found that confined donor is more stable inside ZnTe/CdSe inverted core/shell nanodot than in CdSe/ZnTe core/shell heterodot. Further, the change of confined donors energy against the external magnetic field intensity is detailed in Refs. [9,10]. On the other hand, a recent study [11] reveals that one can modulate the donor binding energy Stark shift by controlling the shell thickness of a core/shell quantum dot.

Further, it is also well-known, that our current knowledge concerning the optical properties of nanomaterials is the fruits of the work achieved by many scientists. For instance, Yesilgul [12] has examined the optical absorption coefficients and refractive index changes of a double semi-V-shaped quantum wells. His paper shows a great change of the total optical coefficient with the incident optical intensity for large barrier width values. The same study was reported by Safarpour and Barati [13] but this time for a system consisting of a spherical InAs nanodot hosted at the center of a GaAs cylindrical quantum wire. Their model gives an ample description on the size dependence of confined systems optical properties. Besides, Çakır and co-workers [14], by the mean of a density matrix formalism, have carried out the total refractive index changes and absorption coefficients in a spherical quantum dot. Their study, provides that the total refractive index change is remarkably enhanced by increasing charge carriers density. In addition, Ref. [15] is a theoretical investigation emphasizing the optical absorption coefficient behavior of a spherical nanodot with parabolic potential. While, the optical properties of quantum disk in the presence of high-frequency laser field are studied by Gambhir et al. [16]. It was found that the laser radiation leads to a significant nonlinear effect on the optical behavior. Further, the impact of an external laser field on the optical characteristics of a parabolic quantum well under an electric field is the subject of Ref. [17]. The authors of this paper have discussed the possibility to control the absorption coefficient and refractive index change by tailoring the laser dressing parameter or again by adjusting the electric field intensity. On the other hand, Mughnetsyan and coworkers [18] have interested in the intraband linear and nonlinear light absorption change with respect to the spin-orbit coupling constant and the hydrostatic pressure. Their results reveal that the increase of the spin-orbit coupling constant leads to a great enhancement of the optical absorption resonant peak magnitude. In addition, a detailed study of the optical characteristics of quantum rings can be found in numerous papers, including [19–22]. However, the examination of the optical behavior of an AlAs/GaAs spherical core/shell nanodots in the presence of a single dopant was the aim of the investigation performed by El Haouari et al. [23]. Besides, taking into account the polaronic effects,

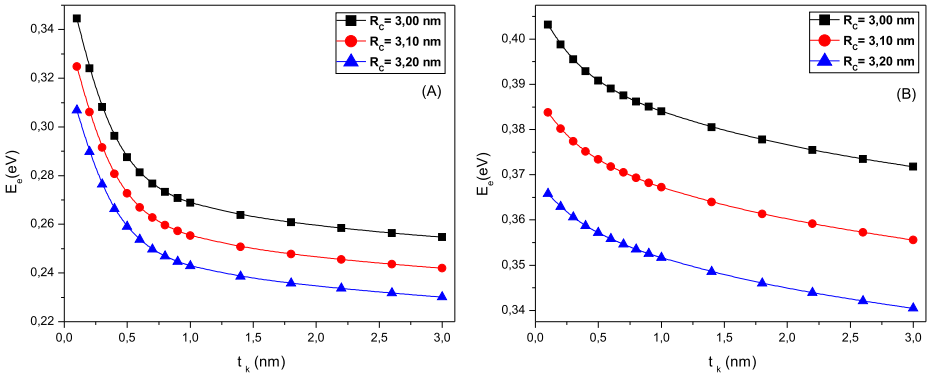

Fig. 2. Electron energy with regard to the shell thickness for various core material size: (A) 1s state and (B) 1p state.

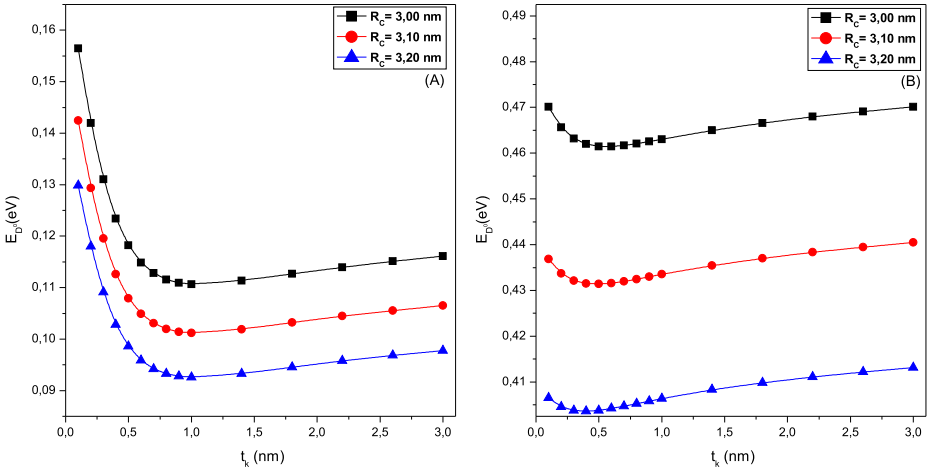

Fig. 3. Total donor energy against the shell thickness for several core material size: (A) 1s state and (B) 1p state.

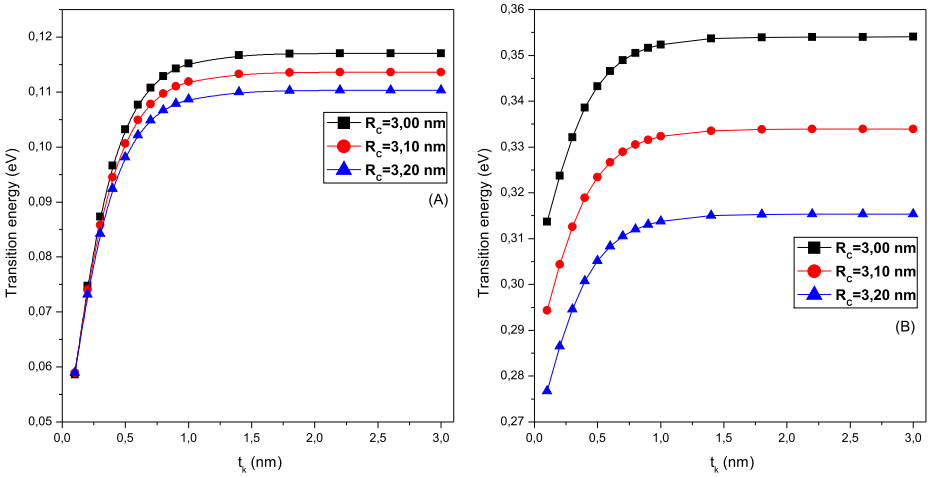

Fig. 4. 1 p– 1s transition energy as a function of the shell thickness for various core radii: (A) Confined electron and (B) Confined donor.

M'zerd and coworkers [24] have examined the impact of the confined donor localization and the heterodot dimensionality on the linear and nonlinear optical characteristics. In addition, using the potential morphing approach in the context of the EMA, Zeng and coworkers [25] have studied the impact of impurity, dielectric environment, and the shell thickness on the optical behavior of ZnS/ZnO and ZnO/ZnS heterodots. Their investigation reveals a great influence of charge carriers localization on the optical characteristics of core/shell nanodots. On the other hand, employing an iterative method within the framework of the compact-density-matrix formalism, and considering an infinite depth potential in the shell region, Zhang et al. [26] have studied the optical properties of a GaAs/AlGaAs spherical nanodot. However, Şahin al. [27] have examined the photoionization cross section related to a centered donor inside a multi-layered spherical heterodot. Besides, Rahul and coworkers [28] have treated the spatial parameters impact on the optical behavior of electrons in a CdS/ZnS/CdS/ZnS multilayer nanodot.

The present theoretical study emphasizes the size control of the optical properties related to centered donors in a CdSe/ZnTe [29–31] core/shell spherical heteronanodot. Through the use of a density matrix formalism, linear and nonlinear OACs and RI changes were investigated. By the way, the 1s-1p donor transition energy was examined by the mean of a variational approach within the framework of the EMA. The following section includes the essential of our used theory, while Section 3 is allocated to the presentation of our obtained numerical results.

2. The applied theory

Let us consider a centered donor in a heteronanodot consisting of a

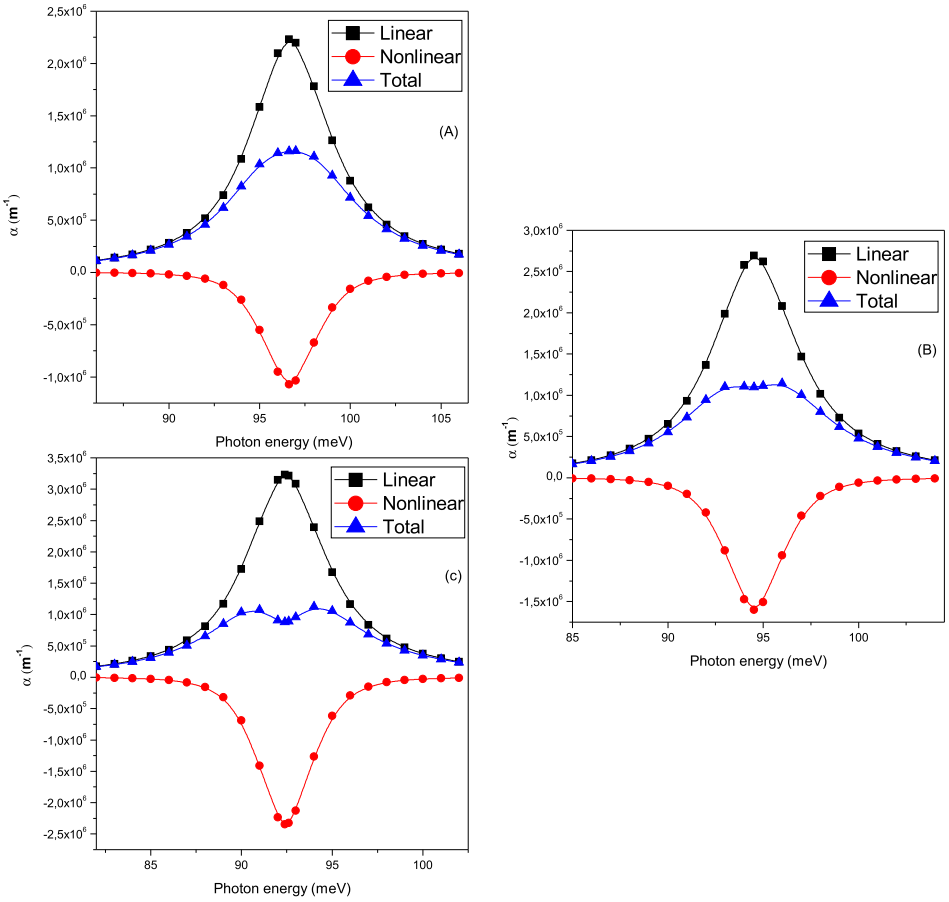

Fig. 5. Electron optical absorption coefficients versus the photon energy, for $I = 210^8$ W·m^{-2}, $t_k = 0.40$ nm and various core size: (A) $R_c = 3.00$ nm, (B) $R_c = 3.10$ nm, and (C) $R_c = 3.20$ nm.

spherical CdSe quantum dot encapsulated by a ZnTe spherical shell. In order to conserve our nanostructure from external medium contaminations, the CdSe/ZnTe nanodot is placed in a silica matrix SiO_2. Fig. 1 schematically illustrates the understudied nanostructure. Where R_c and R_s denote, respectively, the core and shell radii. $U_e = 1.27$ eV refers to the confining potential, while r_{e-D^+} is the electron-impurity distance. Thus, in the context of the EMA, the Schrö dinger equation describing the confined donor energy behavior is given as follow:

$$\left[\Delta_e\left(\frac{-\hbar}{2m_e^*(r)}\right)\Delta_e + U_w(r) + U_{coul.}(r) + \Sigma(R_s)\right]\Phi_{D^0}(r) = E_{D^0}\Phi_{D^0}(r). \tag{1}$$

The first term in the bracket is the kinetic contribution, where the electron effective mass $m_e^*(r)$ is taken to be m_1^* inside the CdSe core and m_2^* in the ZnTe shell, while the second one stands for the confining potential written as:

$$U_w(r) = \begin{cases} 0 & r \leqslant R_c \\ U_e & R_c < r \leqslant R_s. \\ 0, & Otherwise \end{cases} \tag{2}$$

The third and fourth term denote, respectively, the coulomb potential and the self-energy formulated as [32,33]:

$$U_{coul}(r) = -\frac{e^2}{\tilde{\varepsilon} r} - \frac{e^2(\tilde{\varepsilon} - \varepsilon_{out})}{\tilde{\varepsilon}\varepsilon_{out} R_s}, \tag{3}$$

and

$$\Sigma(R_s) = -\frac{e^2}{2R_s}\left[\frac{1}{\tilde{\varepsilon}} - \frac{1}{\varepsilon_{out}}\right] + 0.47\frac{e^2}{\tilde{\varepsilon} R_s}\left[\frac{\tilde{\varepsilon} - \varepsilon_{out}}{\tilde{\varepsilon} + \varepsilon_{out}}\right]. \tag{4}$$

$\tilde{\varepsilon} = \sqrt{\varepsilon_1 \varepsilon_2}$ and $\varepsilon_{out} = 3.9$ [25] are the dielectric constants of the core/shell nanodot and the silica matrix, respectively. It is worth remembering, at this point, that a variational calculations are deployed in order to examine the 1s and 1p donor energies change with regard to the nanodot size. For this purpose, the 1s and 1p donor trial wave functions were taken, in this order, as:

$$\Phi_{D^0}^{1s}(r) = \begin{cases} N_1 \frac{\sin(\kappa_1 r)}{r} e^{-\alpha r} & r \leqslant R_c \\ N_2 \frac{\sinh(\kappa_2 (r - R_s))}{r} e^{-\alpha r} & R_c < r \leqslant R_s, \\ 0 & Otherwise \end{cases} \tag{5}$$

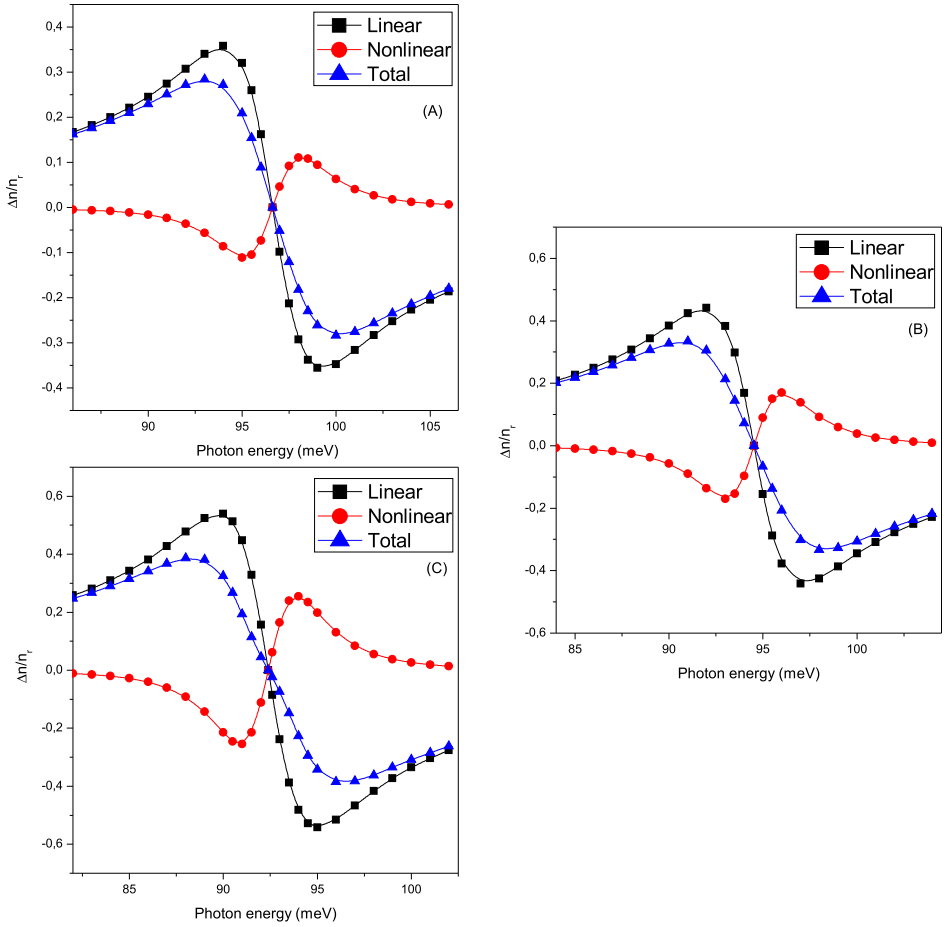

Fig. 6. Electron RI changes as a function of the photon energy, for $I = 210^8$ W·m^{-2}, $t_k = 0.40$ nm and various core size: (A) $R_c = 3.00$ nm , (B) $R_c = 3.10$ nm, and (C) $R_c = 3.20$ nm.

and

$$\Phi_{D^0}^{1p}\left(r,\theta\right) = \begin{cases} N_3 \left[\frac{\sin(\kappa_3 r)}{r} - \cos(\kappa_1 r)\right]\cos(\theta)e^{-\beta r} & r \leqslant R_c \\ N_4 \left[\frac{\sinh(\kappa_4(R_s - r))}{r} + \cosh(\kappa_1(r - R_s))\right]\cos(\theta)e^{-\beta r} & R_c < r \leqslant R_s \\ 0 \quad \textit{Otherwise} \end{cases} \tag{6}$$

where,

$$\kappa_i = \begin{cases} \sqrt{\frac{2m_1^*}{\hbar^2}(E_{nl} - \Sigma(R_s))} & i = 1, 3 \\ \sqrt{\frac{2m_2^*}{\hbar^2}(U_e + \Sigma(R_s) - E_{nl})} & i = 2, 4 \end{cases} \tag{7}$$

$N_j (j = 1 - 4)$ and α, β are, respectively, the normalization constants and the variational parameters. While E_{nl} ($n = 1$ and $l = 1, 0$) stand for confined electron energies. In this connection, the expression of the donor ground state energy is given as follow:

$$E_{D^0} = \min_{\alpha}\left[\frac{\langle\Phi_{D^0}^{1s}(r)|\ H_{D^0}\ |\Phi_{D^0}^{1s}(r)\rangle}{\langle\Phi_{D^0}^{1s}(r)|\Phi_{D^0}^{1s}(r)\rangle}\right], \tag{8}$$

however, the hydrogenic donor lowest excited state reads:

$$E_{D^0} = \min_{\beta}\left[\frac{\langle\Phi_{D^0}^{1p}\left(r,\theta\right)|\ H_{D^0}\ |\Phi_{D^0}^{1p}\left(r,\theta\right)\rangle}{\langle\Phi_{D^0}^{1p}\left(r,\theta\right)|\Phi_{D^0}^{1p}\left(r,\theta\right)\rangle}\right]. \tag{9}$$

H_{D^0} is the donor Hamiltonian already presented.

On the other hand, based on a density matrix approach, one can write the linear and third-order nonlinear optical absorption coefficients, respectively, as [34–36]:

$$\alpha^{(1)}(\omega) = \omega\sqrt{\frac{\mu}{\varepsilon}}\frac{|M_{ij}|^2\hbar\rho_s\Gamma_0}{(E_{fi} - \hbar\omega)^2 + (\hbar\Gamma_0)^2}, \tag{10}$$

and

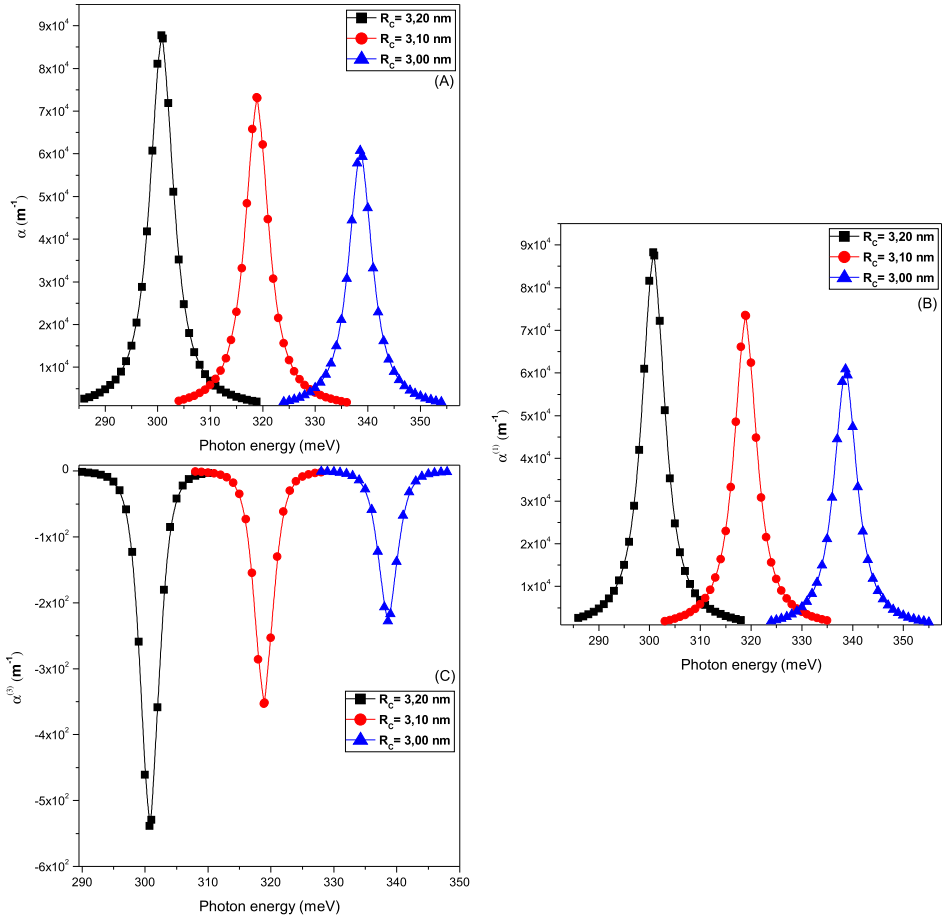

Fig. 7. Donor optical absorption coefficients plotted, for $I = 210^8$ W·m^{-2}, $t_k = 0.40$ nm and various CdTe radii, versus the photon energy: (A) total OAC , (B) linear OAC, and (C) nonlinear OAC.

$$\alpha^{(3)}\left(\omega, I\right) = -\sqrt{\frac{\mu}{\widetilde{\varepsilon}}}\left(\frac{2\omega I}{\varepsilon_0 n_r c}\right)\frac{|M_{ij}|^4 \hbar\rho_s \Gamma_0}{[(E_{fi} - \hbar\omega)^2 + (\hbar\Gamma_0)^2]^2}. \tag{11}$$

where, $\rho_s = 3\,10^{22}$ m^{-3}, Γ_0, n_r, and $E_{fi} = E_f - E_i$ are the charge carriers density, the relaxation rate, the refractive index, and the $1p - 1s$ transition energy respectively. While c stands for the speed of light in vacuum, and I is the incident optical radiation. Further, the electric dipole moment of the transition between i and j states is referred by $M_{ij} = e\langle\Psi_i(\mathbf{r})|\ r\cos(\theta)|\Psi_j(\mathbf{r})\rangle$. Against this background, the total optical absorption coefficient is theoretically formulated as:

$$\alpha(\omega, I) = \alpha^{(1)}(\omega) + \alpha^{(3)}(\omega, I). \tag{12}$$

Likewise, the linear and third-order nonlinear refractive index changes are analytically expressed, in this order as:

$$\frac{\Delta n^{(1)}(\omega)}{n_r} = \frac{\rho_s}{2n_r^2\varepsilon_0}\frac{|M_{ij}|^2 (E_{fi} - \hbar\omega)}{(E_{fi} - \hbar\omega)^2 + (\hbar\Gamma_0)^2}, \tag{13}$$

and

$$\frac{\Delta n^{(3)}(\omega, I)}{n_r} = -\frac{\mu c\rho_s I}{n_r^3\varepsilon_0}\frac{|M_{ij}|^4 (E_{fi} - \hbar\omega)}{[(E_{fi} - \hbar\omega)^2 + (\hbar\Gamma_0)^2]^2}. \tag{14}$$

where μ denotes the permeability of the understudied system. In this context, the total refractive index change is given as follow:

$$\frac{\Delta n^{(3)}(\omega, I)}{n_r} = \frac{\Delta n^{(1)}(\omega)}{n_r} + \frac{\Delta n^{(3)}(\omega, I)}{n_r}. \tag{15}$$

3. Numerical results

Reminding, at this spot, that in order to simplify our numerical calculations, reduced units were deployed by defining $\overline{R}_{D^0} = \frac{\hbar^2}{2\widetilde{m}_e^* \bar{a}_{D^0}^2} = 18.478$ meV as unit of energy and $\bar{a}_{D^0} = \frac{\widetilde{\varepsilon}\hbar^2}{e^2\widetilde{m}_e^*} = 3.842$ nm as unit of length. By the way, Table 1 provides the various used physical parameters.

Fig. 2, shows the variation of the electron energy, related to $1s$ (A) and $1p$ states (B), with regard to the shell thickness, $t_k = R_s - R_c$, for

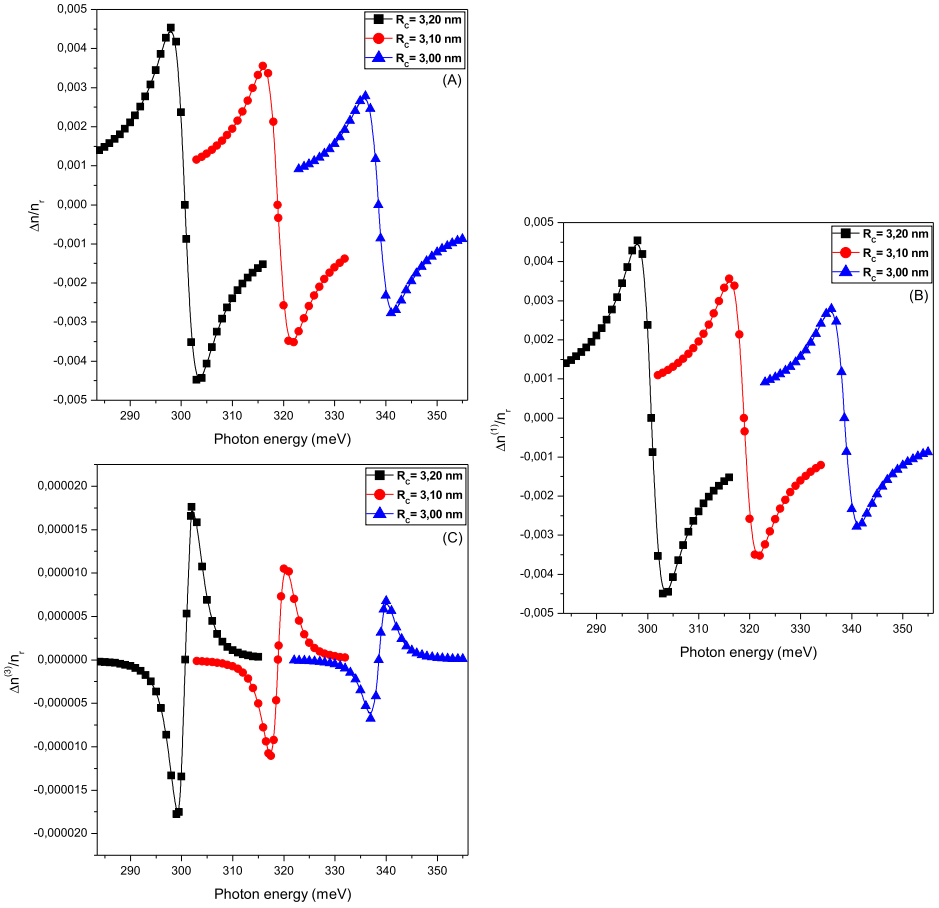

Fig. 8. Donor RI changes, for $I = 210^8$ W·m^{-2}, $t_k = 0.40$ nm and various CdTe radii, with respect to the photon energy: (A) total RI change, (B) linear RI change, and (C) nonlinear RI change.

various core material size. It is noticeable that the change of the shell thickness as well as the core size have remarkable impacts on the 1s and 1p electron energies. Then again, and as expected, the 1p electron energy values are greater than those of the 1s state. It was also found that the electron energy, for both 1s and 1p states, is blue-shifted when the size of the core or the shell materials is reduced. Further, one can observe that, for a fixed core radius, the electron ground state energy increases by about 82 meV when the shell thickness moves from 3 nm to 0.1 nm, while the 1p electron energy is virtually increases by 29 meV. Accordingly, one can assume that the 1s electron energy is more sensitive to the change of the shell thickness than the lowest first excited state.

In Fig. 3, the 1s (A) and 1p (B) donor energies were depicted as a function of the shell thickness for different core radii $R_c = 3.00$ nm, 3.10 nm, 3.20 nm. It was established that 1s and 1p donor energies are the subject of a great increase when the core radius is shrunk. However, it was found that the donor energy is red-shifted by increasing the shell thickness up to a critical thickness value, $t_k = 1.00$ nm (0.50 nm) for 1s (1p) state, after that a remarkable increase of the 1s and 1p impurity energy states is assisted.

Fig. 4, presents the 1p to 1s transition energy, related to electrons (A) and donors (B), against the ZnTe thickness, for various CdSe radii $R_c = 3.00$ nm, 3.10 nm, 3.20 nm. It is worth noticing that for very small shell thickness, less than 0.20 nm, the electron transition energy is practically not affected by the nanodot size. On the other hand, decreasing the core material size leads to increase the electron transition energy for nandots with shell thickness greater than 0.20 nm. The same effect is observed, for a fixed core radius, when the shell thickness increases up to $t_k \simeq 1.30$ nm. Otherwise, the electron transition energy becomes virtually constant. One can also see, that the presence of donors blue-shifts the transition energy and makes this physical entity sensitive to the core material size even for very small values of the shell thickness. Furthermore, it was established that, for t_k greater than 1.30 nm, the donor transition energy is practically not affected by the variation of the shell thickness.

Additionally, the linear, nonlinear and total electron optical absorption coefficients as a function of the photon energy, for $I = 210^8$ W·m^{-2}, $t_k = 0.40$ nm and various core size $R_c = 3.00$ nm (A), 3.10 nm (B), 3.20 nm (C), are displayed in Fig. 5. Obviously, one can observe that the electron OACs have significant values only for photon

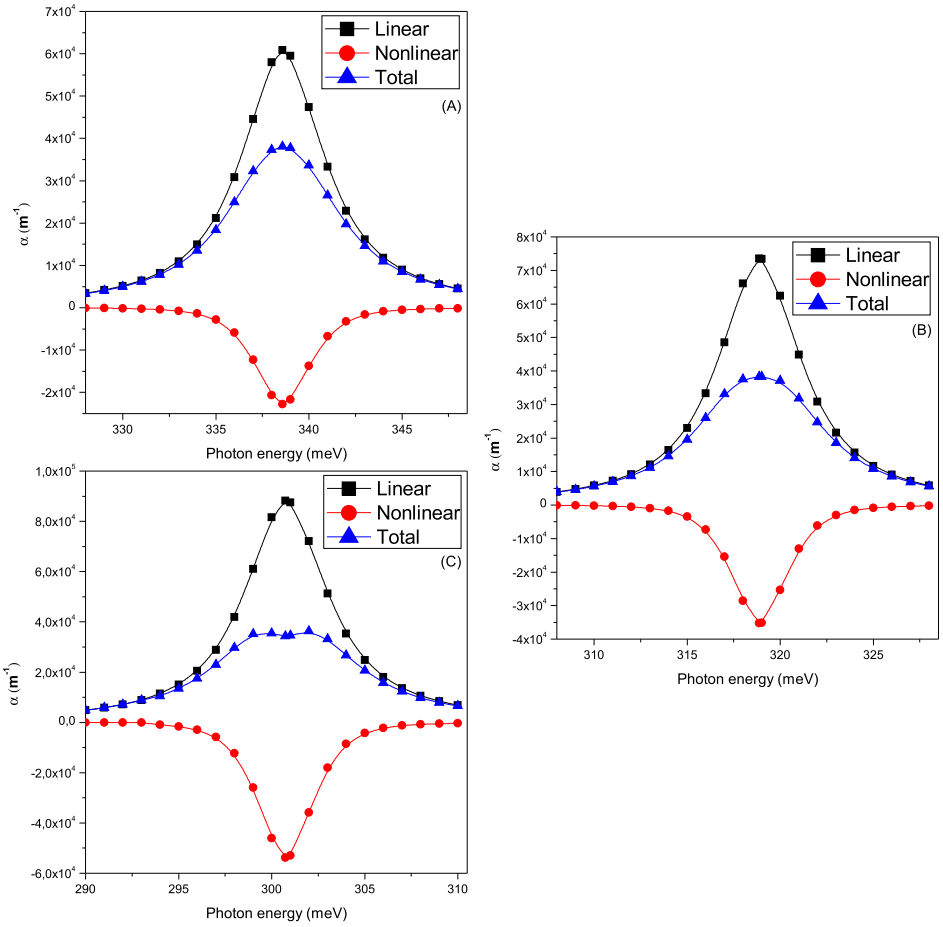

Fig. 9. Donor optical absorption coefficients against the photon energy, for $I = 210^{10}$ W·m^{-2}, $t_k = 0.40$ nm and several core radii: (A) $R_c = 3.00$ nm , (B) $R_c = 3.10$ nm, and (C) $R_c = 3.20$ nm.

energies around the threshold 1p to 1s transition energy. It was also found that, for a fixed ZnTe thickness, the amplitude of the linear and nonlinear OAC resonance peaks decreases with decreasing the CdSe size. Nevertheless, the total electron OAC resonance peak magnitude increases by reducing the core material size. It was established, furthermore, that increasing the core radius leads to a split of the resonance peak into two symmetric peaks. On the other hand, a blueshift of the electron OAC peaks position is assisted when the core material size is decreased.

Fig. 6, exhibits the linear, nonlinear and total electron RI changes against the photon energy, for $I = 210^8$ W·m^{-2}, $t_k = 0.40$ nm and various core size $R_c = 3.00$ nm (A), 3.10 nm (B), 3.20 nm (C). It is noticeable that the nonlinear contribution of the RI change impacts the quantitative behavior of the total RI change. On the other hand, it was obtained that the magnitude of the total RI change is reduced when the core material radius moves from 3.20 nm to 3.00 nm.

In Fig. 7, taking $I = 210^8$ W·m^{-2} and $t_k = 0.40$ nm, the total (A), linear (B) and nonlinear (C) optical absorption coefficients of donors are plotted versus the photon energy considering various CdSe radii. It is quite clear that, the presence of impurities considerably reduces the magnitude of the optical absorption coefficients of our core/shell heterodot. By contrast, the core/shell OAC peaks position are blueshifted when impurities effects are considered. Additionally, our model reveals that, for the considered physical parameters, increasing the core material leads to increase the magnitude of the OAC resonance peaks. That might be related to the poor contribution of the nonlinear term in the total AOC.

In Fig. 8, the total (A), linear (B) and nonlinear (C) RI changes are drawn as a function of the photon energy for several core radii. Our results, performed under the same condition as in Fig. 7, exhibit a noticeable redshift of the RI changes peaks when the core radius increases. However, it was obtained, that decreasing the core size is associated to a great diminishing of the RI changes magnitude. Additionally, one can also observe that the nonlinear RI change magnitude is so small in such a way that its contribution can be marginalized.

Fig. 9, illustrates the linear, nonlinear and total donor optical absorption coefficients versus the photon energy, for $I = 210^{10}$ W·m^{-2}, $t_k = 0.40$ nm and various core size $R_c = 3.00$ nm (A),

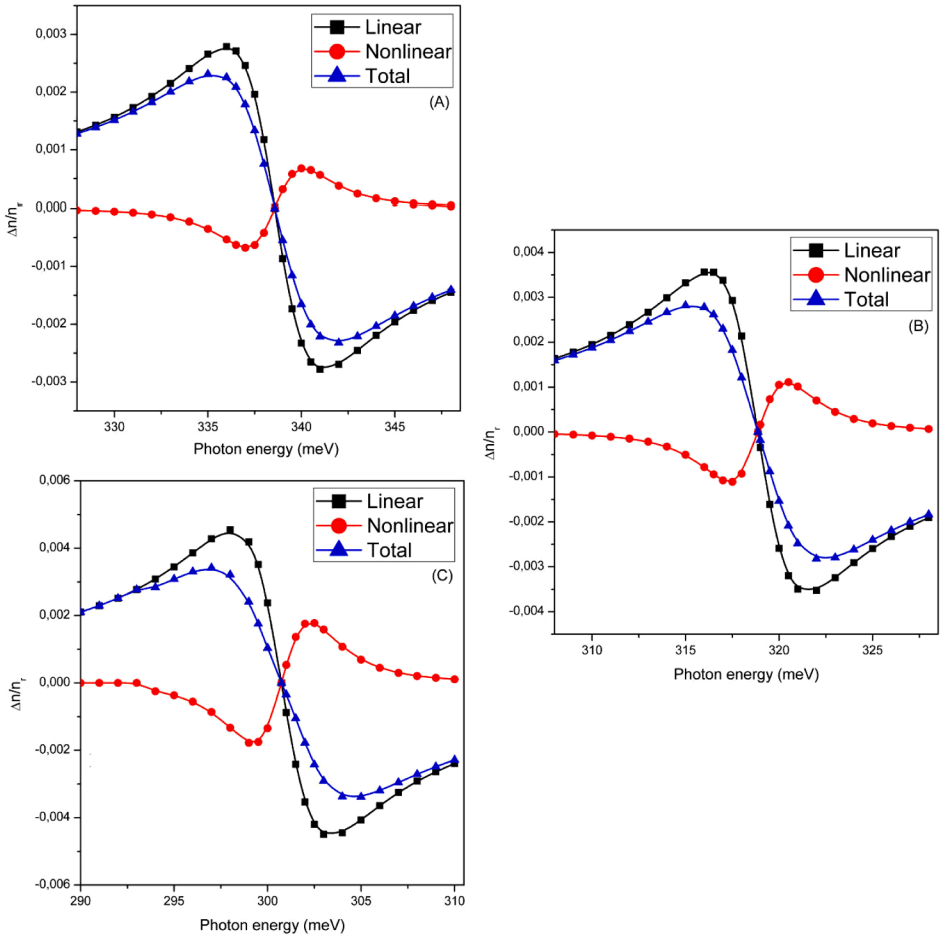

Fig. 10. Donor RI changes versus the photon energy, for $I = 210^{10}$ W·m^{-2}, $t_k = 0.40$ nm and various core radii: (A) $R_c = 3.00$ nm , (B) $R_c = 3.10$ nm, and (C) $R_c = 3.20$ nm.

3.10 nm (B), 3.20 nm (C). Qualitatively, the situation seems to be similar to that in Fig. 7 and the same conclusions can be pointed out. By contrast, it was found that the increase of the incident optical radiation intensity results in a remarkable increase of the nonlinear OAC magnitude. That, automatically, leads to a decrease of the total OAC resonance peak magnitude. Further, it was established that when the core radius moves from 3.20 nm to 3.10 nm a slight increase of the total OAC resonance peak amplitude is observed. However, the magnitude of the total OAC resonance peak undergoes a remarkable decrease when R_c moves from 3.10 nm to 3.00 nm.

Fig. 10, presents the linear, nonlinear and total RI changes against the photon energy, for $I = 210^{10}$ W·m^{-2}, $t_k = 0.40$ nm and several core radii $R_c = 3.00$ nm (A), 3.10 nm (B), 3.20 nm (C). One can remark that increasing the intensity of the optical radiation leads to decrease the magnitude of the total RI change. That is explained by the competition between the linear and nonlinear RI changes, since the fact that the decrease of the optical radiation leads to decrease the nonlinear RI change.

Fig. 11, shows the linear, nonlinear and total donor optical absorption coefficients with respect to the change of the photon energy, for $I = 210^{8}$ W·m^{-2}, $t_k = 1.00$ nm and various core size $R_c = 3.00$ nm (A), 3.10 nm (B), 3.20 nm (C). As compared with Fig. 7, it is obvious that the rise of the shell thickness is associated with an enhancement of the optical absorption coefficients magnitude. In addition, one can also notice that the nonlinear contribution has a great impact on the total OAC. Furthermore, it was shown that the increase of t_k blueshifts the optical absorption coefficients resonance peak position. Otherwise, the change of the optical absorption coefficients with respect to the photon energy is the same as in Fig. 7.

In Fig. 12, the linear, nonlinear and total RI changes are presented

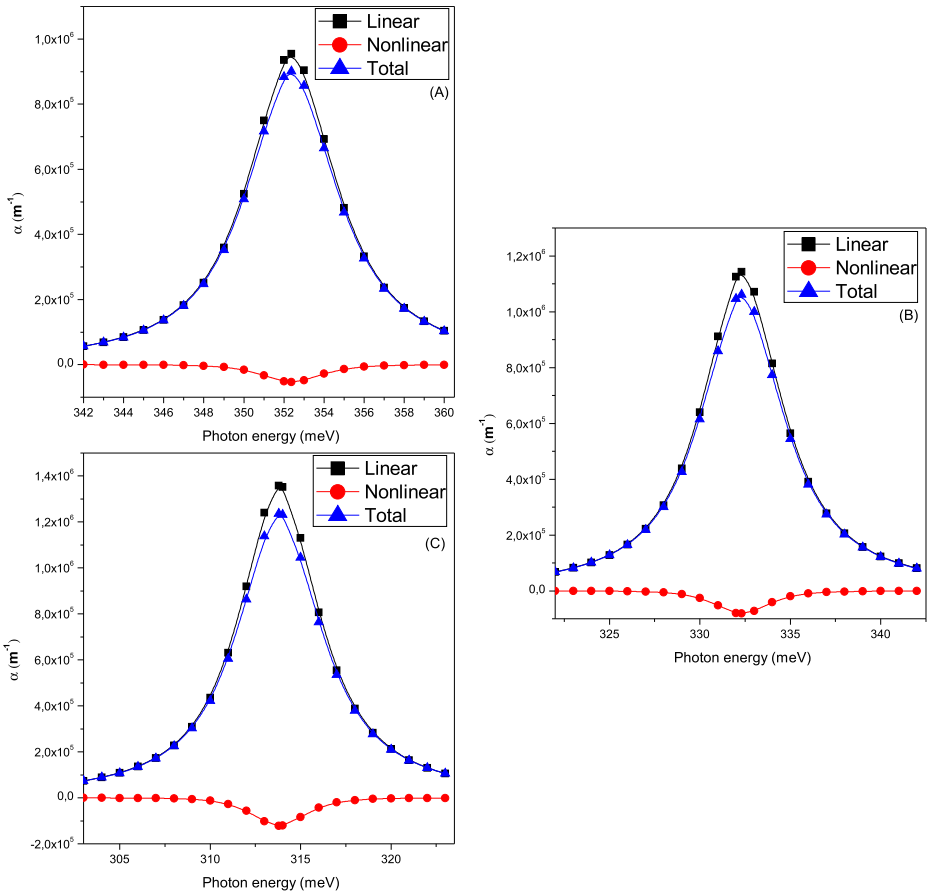

Fig. 11. Donor optical absorption coefficients as a function of the photon energy, for $I = 210^8$ W·m^{-2}, $t_k = 1.00$ nm and several core radii: (A) $R_c = 3.00$ nm , (B) $R_c = 3.10$ nm, and (C) $R_c = 3.20$ nm.

with respect to the variation of the photon energy, for $I = 210^8$ W·m^{-2} , $t_k = 1.00$ nm and different core size $R_c = 3.00$ nm (A), 3.10 nm (B), 3.20 nm (C). Our theoretical results reveal a remarkable increase of the RI changes magnitude by increasing the shell thickness. Additionally, one can also remark that the nonlinear RI contribution still very poor, virtually, as in Fig. 8. On the other hand, RI changes peaks position are found to be blueshifted by increasing t_k.

4. Conclusion

In short, our theoretical study highlights the size impact on the optical properties of electrons and donors inside a spherical core/shell heterodot (SCSHD). Further, the influence of the incident optical radiation was also discussed. Our used theory, based on a combination between a density matrix approach and a variational calculations, reveals the possibility to modulate the refractive index changes and the optical coefficients by the control of the spatial parameters of the understudied system. Namely, it was obtained that the total RI change magnitude decreases with decreasing the nanodot spatial parameters. On the other hand, it was established that the increase of the incident optical radiation intensity reduces the magnitude of the RI change. In addition, it was found that the reduction of the heteronanodot size is not always related to the enhancement of the donor total OA resoance peak magnitude. By contrast, decreasing the nanodot size leads to increase the electron total OA resoance peak magnitude. However, the RI changes and the optical absorption coefficients peaks positions are found to be redshifted by increasing the core radius or by decreasing the shell thickness.

Acknowledgments

This work has been initiated with the support of URAC: 08, the project PPR2: (MESRSFC-CNRST) and the Swedish Research Links program dnr-348-2011-7264 and completed during a visit of A. A at the Max Planck Institut für Physik Komplexer Systeme Dresden, Germany. The authors would like to thank all the organizations.

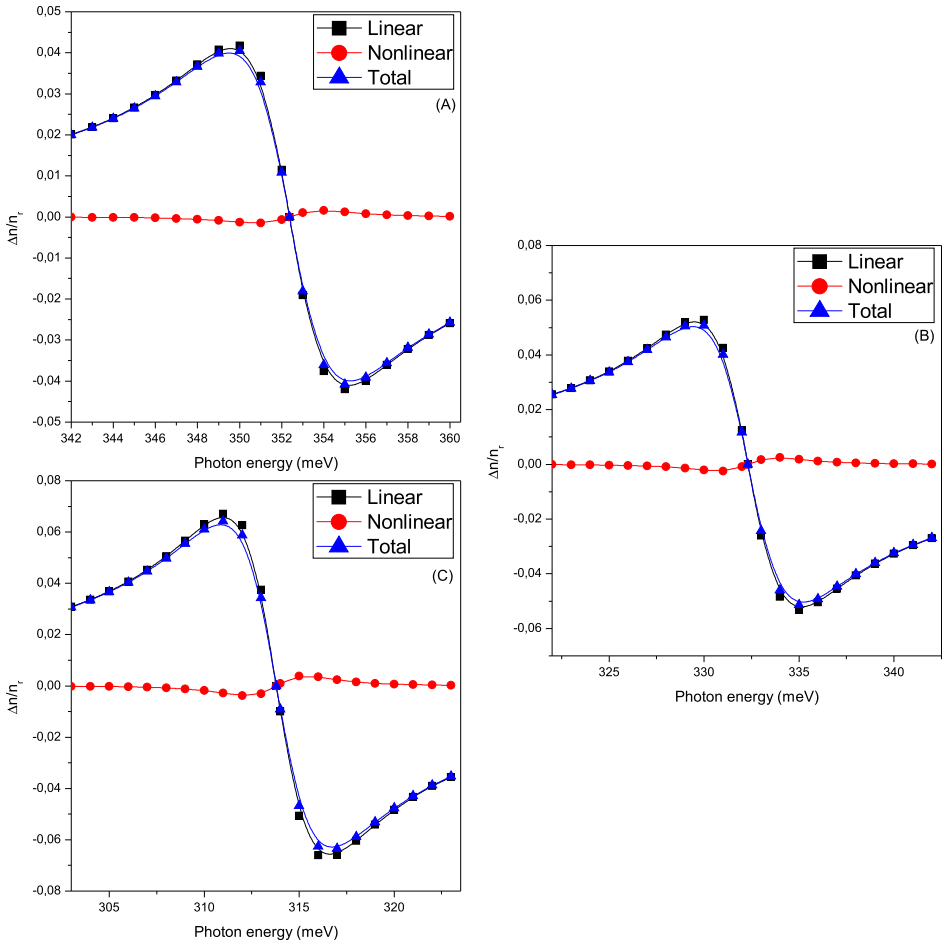

Fig. 12. Donor RI changes against the photon energy, for $I = 210^8$ W·m^{-2}, $t_k = 1.00$ nm and several core radii: (A) $R_c = 3.00$ nm , (B) $R_c = 3.10$ nm, and (C) $R_c = 3.20$ nm.

Appendix A. Supplementary data

Supplementary data associated with this article can be found, in the online version, athttps://doi.org/10.1016/j.rinp.2019.102414.

References

[1] Cristea M. Physica E 2018;103:300.
[2] de Souza GVB, Bruno-Alfonso A. Physica E 2015;66:128.
[3] Causil DA, Beltrán CL, Villamil P. Physica E 2015;74:510.
[4] Boz FK, Nisanci B, Aktas S, Okan SE. Appl Surf Sci 2016;387:76.
[5] Stojanović D, Kostić R. Opt Quant Electron 2016;48:226.
[6] Kes H, Bilekkaya A, Aktas S, Okan SE. Superlattices Microstruct 2017;111:966.
[7] El Haouari M, Feddi E, Dujardin F, Restrepo RL, Mora-Ramos ME, Duque CA. Superlattices Microstruct 2017;111:457.
[8] Chafai A, Dujardin F, Essaoudi I, Ainane A, Ahuja R. Superlattices Microstruct 2017;111:976.
[9] Chafai A, Essaoudi I, Ainane A, Dujardin F, Ahuja R. Physica E 2017;94:96.
[10] Chafai A, Essaoudi I, Ainane A, Dujardin F, Ahuja R. Chin J Phys 2019;57:189.
[11] Chafai A, Essaoudi I, Ainane A, Dujardin F, Ahuja R. Physica E 2018;104:29.
[12] Yesilgul U. J Lumin 2012;132:765.
[13] Safarpour G, Barati M. J Lumin 2013;137:98.
[14] Çakír B, Yakar Y, Özmen A. J Lumin 2012;132:2659.
[15] Yakar Y, Çakír B, Özmen A. Opt Commun 2010;283:1795.
[16] Gambhir M, Kumar M, Jha PK, Mohan M. J Lumin 2013;143:361.
[17] Yesilgul U, Ungan F, Sakiroglu S, Mora-Ramos ME, Duque CA, Kasapoglu E, Sarí H, Sökmen I. J Lumin 2014;145:379.
[18] Mughnetsyan VN, Manaselyan AKh, Barseghyan MG, Kirakosyan AA. J Lumin 2013;134:24.
[19] Ghajarpour-Nobandegani S, Karimi MJ. Opt Mater 2018;82:75.
[20] Baghramyan HM, Barseghyan MG, Kirakosyan AA, Restrepo RL, Mora-Ramos ME, Duque CA. J Lumin 2014;145:676.
[21] Duque CM, Acosta RE, Morales AL, Mora-Ramos ME, Restrepo RL, Ojeda JH, Kasapoglu E, Duque CA. Opt Mater 2016;60:148.
[22] Bejan D, Stan C, Niculescu EC. Opt Mater 2018;78:207.
[23] El Haouari M, Talbi A, Feddi E, El Ghazi H, Oukerroum A, Dujardin F. Opt Commun 2017;383:231.
[24] M'zerd S, El Haouari M, Talbi A, Feddi E, Mora-Ramos ME. J Alloys Compd 2018;753:68.
[25] Zeng Z, Garoufalis CS, Terzis AF, Baskoutas S. J Appl Phys 2013;114:023510.
[26] Zhang ZH, Zhuang G, Guo KX, Yuanc JH. Superlattices Microstruct 2016;100:440.
[27] Şahin M, Tek F, Erdinç A. J Appl Phys 2012;111:084317.
[28] Rahul SK, Snehaa AK, Mathew V. Superlattices Microstruct 2019;129:1.
[29] Kaniyankandy S, Rawalekar S, Verma S, Ghosh HN. J Phys Chem C 2011;115:1428.
[30] Liu Y, Zhang C, Zhang H, Wang R, Hua Z, Wang X, Zhang J, Xiao M. Adv Mater 2013;25:4397.
[31] Rai SC, Wang K, Chen J, Marmon JK, Bhatt M, Wozny S, Zhang Y, Zhou W. Adv Electron Mater 2015;1:1400050.
[32] Allan G, Delerue C, Lannoo M, Martin E. Phys Rev B 1995;52:11982.
[33] Chafai A, Essaoudi I, Ainane A, Dujardin F, Ahuja R. Physica E 2018;101:125.
[34] Ünlü S, Karabulut İ, Şafak H. Physica E 2006;33:319.
[35] Baskoutas S, Garoufalis C, Terzis AF. Eur Phys J B 2011;84:241.
[36] Karabulut İ, Baskoutas S. J Appl Phys 2008;103:073512.
[37] Klimov VI. Nanocrystal quantum dots. CRC Press; 2010.
[38] Borisenko VE, Ossicini S. What is what in the nanoworld. Wiley-VCH Verlag & Co. KGaA; 2012.